RSC Advances

PAPER

View Article Online
View Journal | View Issue

Cite this: *RSC Adv.*, 2017, **7**, 2

Surface and interface structural analysis of W deposited on 6H–SiC substrates annealed in argon

T. T. Thabethe,*[a] E. G. Njoroge,[a] T. T. Hlatshwayo,[a] T. P. Ntsoane[b] and J. B. Malherbe[a]

A study of a tungsten (W) thin film deposited on a single crystalline 6H–SiC substrate and annealed in Ar at temperatures of 700 °C, 800 °C, 900 °C and 1000 °C for 1 hour was conducted. The subsequent solid state reactions, phase composition and surface morphology were investigated by Rutherford backscattering spectrometry (RBS), grazing incidence X-ray diffraction (GIXRD) and scanning electron microscopy (SEM) analysis techniques. RBS analysis of as-deposited samples indicated the presence of W and oxygen in the as-deposited thin film, the GIXRD analysis of the as-deposited film showed the presence of W, WO_3, W_5Si_3 and WC. RBS results of the sample annealed at 700 °C indicated interaction between W and SiC with the formation of a reaction zone. The GIXRD analysis indicated the presence of W_5Si_3, WO_3, SiO_2, W_2C and WC in the W–SiC reaction zone (RZ) after annealing at 700 °C. At temperatures of 800 °C to 1000 °C, the W–SiC samples did not show any new phase formation from the GIXRD patterns, while the RBS results indicate an increase in the RZ width which meant further reactions were taking place. An increase in the peak intensities of the GIXRD patterns was observed due to a change in the polycrystalline nature of the W film to a more crystalline structure. SEM micrographs of the as-deposited samples indicated that the W thin film had a uniform surface with small grains. Annealing at 700 °C and above led to the formation of large crystals. The large crystals formed were randomly orientated; it was observed that an increase in annealing temperature led to an increase in the film crystal size forming pores between crystals.

Received 6th October 2016
Accepted 16th November 2016

DOI: 10.1039/c6ra24825j

www.rsc.org/advances

1. Introduction

Tungsten (W) is a high melting point metal[1] that is often used in coating or alloyed with other metals to increase their strength. W coatings/alloys are frequently used in many applications because they tend to be strong and flexible, resist wear (wear-resistant parts), resist corrosion, conduct electricity well, *etc.*[2] Due to its stability at high temperatures and heat resistance properties, W is also used in a number of high temperature applications.[3] Some other applications include arch-welding electrodes and heating elements in high-temperature furnaces.[3]

Silicon carbide is one of the materials used in a vast number of applications such as a wide band-gap semiconductor,[4,5] nuclear material,[6–8] reinforced composite,[9] *etc.* This is because of its exceptional properties like high corrosion resistance, high thermal stability, high thermal conductivity, high breakdown electric field strength, *etc.* SiC is used in high power electronic devices which have the ability to operate at temperatures as high as 600 °C.[10] The stability of contacts made between SiC and metals determine the reliability and device performance. One of the metals used for contacts is W due to its properties like low contact resistivity and high thermal stability for ultra-high-large-scale integrations (ULSI) and very-large-scale integrations (VLSI).[11,12] The fabrication of W–SiC ohmic contacts plays a major role in semiconductor applications.

In high temperature gas cooled reactors (HTGR), SiC is used as the main barrier of fission product (FPs) escape. It is used in the tri-structural isotropic (TRISO) fuel particle to encapsulate the UO_2 and ThO_2 fuel kernels.[13,14] SiC is effective in preventing the escape of the FPs with the exception of silver (Ag) and degradation of the SiC by palladium (Pd) and zirconium (Zr).[14–18] An additional protective layer of tungsten is proposed to cover the SiC and probably reduce the interaction of FPs with SiC.[6,19,20]

Rogowski and Kubiak[7] investigated the dependence of electrical properties of W contacts on SiC, the structure and chemical composition of the contacts at the interface during annealing. The resulting initial phases after annealing in Ar ambient were W_5Si_3 and WSi_2. A smooth surface layer with a well-defined continuous W layer was observed on the as-deposited samples, a rough surface (non-uniform) with the formation of pores was reported after annealing. The interaction of W–SiC leading to the formation of silicides and carbides at the interface was also observed by other researchers.[9,21–23]

We have done a detailed study of pure W–SiC annealed in an inert gas, namely, Ar, to understand W–SiC contact behaviour

[a]*Department of Physics, University of Pretoria, Pretoria, 0002, South Africa. E-mail: Thabsile.Thabethe@up.ac.za; Tel: +27 12 420 4510*

[b]*South African Nuclear Energy Corporation SOC Limited, Pretoria 0001, South Africa*

and interface structural changes due to heat treatment. As outlined above, this study is important for both electronic applications (stability W–SiC contacts) and HTGRs application (applied as a diffusion barrier for SiC). Annealing in Ar ambient is mainly used in semiconductor applications for studying electrical properties of W–SiC contacts after thermal annealing.[4] Studies on W–SiC contacts do not take into account the effect of argon annealing on the microstructure of the material and the phases that forms. The reason for the present study is to observe how the material behaves (*i.e.* the initial reaction, phases formed and effect on the surface microstructure) when annealed in an Ar atmosphere.

2. Experimental procedure

Semi-insulating 6H–SiC single-crystal wafers, of 2 inch diameter, 330 μm thickness, with a micro pipe density < 10 cm^{-2} and root mean square (RMS) surface roughness of <0.5 nm were used as starting material. A thin film of W, of about 65 nm was sputter deposited on the 6H–SiC wafers. The details on how this was done are available in ref. 24. The samples were subsequently annealed in argon (Ar) of 99.9% purity atmospheres at 700 °C, 800 °C, 900 °C and 1000 °C for 1 hour. The flow rate of Ar in the quartz tube was maintained at 350 SCCM. This temperature range was chosen because the reaction between W–SiC is expected to occur around 700 °C,[4] this allows us to be able to study the effect caused by the reaction and changes in the structure.

The samples were characterised by Rutherford backscattering spectrometry (RBS) before and after annealing. Simulation of RBS spectra was done using the RUMP code[25] to obtain the thickness and composition of the deposited layer, and the composition of the reaction zone (RZ). The energy used for the He^+ ions was 1.6 MeV with a scattering angle of 165°. Grazing incidence X-ray diffraction (GIXRD) analysis was performed using a Bruker D8 Discover XRD system with a Cu K_α radiation source (1.54184 Å) at two-theta step size of 0.04°. This was done to identify the phases formed and orientation before and after annealing of the samples using the International Centre for Diffraction Data files (ICDD-PDF-2) database. Field emission gun scanning electron microscopy (FEG-SEM) with a Zeiss Ultra 55 high resolution field emission microscope was used to study the surface morphology of the samples before and after annealing at the different temperatures.

3. Results and discussion

3.1. Rutherford backscattering spectrometry (RBS)

The W–SiC samples were annealed in argon ambient from 700 °C to 1000 °C and the resulting RBS results are shown in Fig. 1. The as-deposited RBS spectrum which was simulated using RUMP is available in ref. 24. The as-deposited sample was composed of W and oxygen in the layer (this indicated the presence of an oxide in the deposited layer) and SiC as the substrate. The deposited W thin film layer thickness was about 65 nm (about 412 × 10^{15} atoms per cm^2). The oxygen present on the samples might have been attained during deposition in the

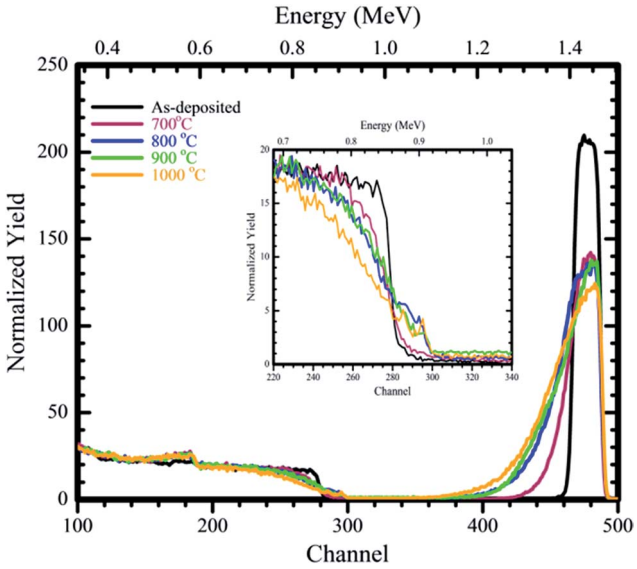

Fig. 1 RBS spectra of the as-deposited and samples annealed in Ar ambient gas for 1 hour at temperatures of 700 °C to 1000 °C and the insert of magnified Si edge from channel numbers 220 to 340.

deposition chamber. The W back edge and Si edge were flat indicating that no reactions took place between W–SiC during deposition. The RBS spectrum of the sample annealed at 700 °C resulted in a reduction in the W peak height and a significant shift of W signal back edge towards lower energy channels. On the Si peak the top edge of the Si signal shifts to lower energy channels and the bottom edge shifts to higher energy channels. These indicated that interdiffusion between W and SiC was taking place. This interdiffused region we call the reaction zone (RZ).

According to the RUMP simulations interdiffusion occurred upon annealing at 700 °C and the calculated RZ width was around 870 × 10^{15} atoms per cm^2. The drastic decrease in height and increase in width of the W peak compared to the as-deposited is attributed to the reaction which took place between W and SiC. The oxygen observed on the as-deposited layer was found to be present at the W–SiC RZ after annealing at 700 °C. What is also evident in Fig. 1 is that the oxygen tails towards the bulk after annealing at 700 °C, which indicates that it is diffusing (moving) towards SiC and it takes part in the reactions taking place between W and SiC.

Annealing at 800 °C resulted in a further shift of the top of the Si edge to lower energy channel numbers, with a step appearing at the bottom of the Si edge. The step is due to the diffusion of Si towards the W film and react to form a RZ which increased in width with temperature increase. A small reduction in the W peak height, accompanied by an increase in the width of W peak (W peak tailed to the lower energy channel numbers, further away from the 700 °C peak) occurred. This indicated that the reaction between W and SiC was continuing to take place with an increase in the RZ width to about 1060 × 10^{15} atoms per cm^2. Annealing at 900 °C resulted in further shift of the W peak to lower energy channel numbers. The peak height of the W peak also reduced when compared to the 800 °C spectrum, while the Si

edge and W peak height showed no noticeable change. The width of the RZ after annealing at 900 °C was about 1220 × 10^{15} atom per cm^2.

Increasing the annealing temperature to 1000 °C resulted to further shift in the Si top edge to lower energy channel numbers and a reduction in the W peak height accompanied by broadening of the W signal towards lower energy channel number. The RZ increased to about 1530 × 10^{15} atoms per cm^2 at 1000 °C. In all the chosen annealing temperatures the oxygen peak was observed to move towards the lower energy channels with the increase in annealing temperature. This indicated that oxygen was taking part in the W–SiC RZ as one of the reacting agents. According to the RUMP simulations, the RZ after annealing from 700 °C to 1000 °C was composed of W, Si, C and O. The possible compounds formed are: tungsten silicide, tungsten carbide, tungsten oxide and silicon oxide. The exact stoichiometries of these compounds are difficult to determine accurately with RBS/RUMP.

Comparing our RBS results above with previous work[24,26] we found the following: initial interface reactions for the vacuum annealed samples occurred at 850 °C, while in H_2 and Ar ambients it occurred at 700 °C. Thus, annealing in Ar and H_2 ambients leads to a lower reaction temperature between W and SiC. Annealing in an Ar ambient leads to higher reaction rate between W and SiC compared to the H_2 ambient and vacuum annealing. The oxygen present does not reduce after annealing the samples in Ar ambient instead it takes part in the reaction; this might also be a reason for the high reaction rate observed in Ar atmosphere. In H_2 ambient, oxygen was removed, remaining a pure tungsten layer. Vacuum annealing indicated reduction in the oxygen with increase in annealing temperature.

3.2. Grazing incident X-ray diffraction (GIXRD)

To confirm the RBS results, GIXRD analysis was consequently done on the samples. The GIXRD patterns of the W thin film deposited on 6H–SiC substrate before and after annealing are depicted in Fig. 2. The resulting XRD patterns of the as-deposited samples are broad indicating that the as-deposited W layer was composed of nano-crystallites. The as-deposited pattern had W peaks with 2θ positions of 43.48°, 57.12° and 72.78° attributed to (211), (200) and (211) reflections respectively. W_5Si_3 peaks assigned to (310) and (512) reflections at 29.49° and 61.57° were also observed. The carbide formed was WC corresponding to (100) and (101) reflections at the 2θ positions 35.55° and 48.38° respectively. This implied that the as-deposited W–SiC sample reacted during deposition resulting in the formation of silicides and carbides. The occurrence of WO_3 with the orientations of ($\bar{1}$40) at 49.02°, (400) at 50.10° and (002) at 51.17° indicated the presence of an oxide in the as-deposited W film. The GIXRD results for the as-deposited sample thus correlate with the RBS results which indicated the presence of oxygen in the W layer. The silicides and carbides were not detected by RBS because their small quantities were below the detection limit of RBS.

Annealing the W–SiC sample at 700 °C resulted in the formation of new peaks as seen in Fig. 2, indicting further reaction between W–SiC took place after annealing at this

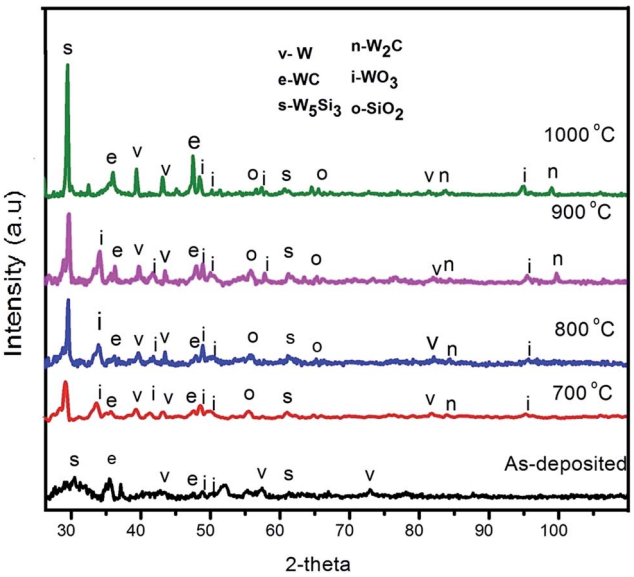

Fig. 2 X-ray diffraction patterns for the as-deposited W–SiC sample and after annealing in argon ambient at 700 °C, 800 °C, 900 °C and 1000 °C for 1 h.

temperature. These results correlate with the RBS results. New peaks indexed to W (101) at position 39.39° and W (222) at 81.19° were observed. It is most likely that they were not observed on the as-deposited because of the nano-particle size nature of the material. WO_3 (112) at 34.26°, (111) at 41.87° and (510) at 95.98° also appeared after annealing at this temperature. The appearance of a SiO_2 peak at 2θ position of 56.85° with the orientation of (535) located at the W and SiC interface was observed after annealing at 700 °C. The formation of SiO_2 on top of SiC could be due to a reaction between WO_3 and SiC. As reported from our RUMP simulations of RBS results, O_2 was found at the RZ layer that formed between W and SiC. Another carbide phase, namely, W_2C with orientation of (103) was formed at 84.39° 2θ position.

The GIXRD pattern for the sample annealed at 800 °C does not show much of a difference from the 700 °C pattern, with a new SiO_2 (404) peak observed at position 65.36°. After annealing at 900 and 1000 °C, a W_2C (203) peak appeared at 97.86° 2θ position. The W_5Si_3, WC, WO_3 and W broad peaks observed on the as-deposited patterns narrowed and increased in intensity upon annealing at 700 °C to 1000 °C, indicating a change in the structure (*i.e.* the sample had large crystals from their polycrystalline nature and change in crystal size) of the sample during annealing. Table 1 shows the calculated grain sizes of the phases observed from Scherrer equation. It can be seen that the crystal sizes of the W_5Si_3, WC, SiO_2 and WO_3 phases increased with annealing temperature. The increase in crystal sizes indicated phase nucleation, which resulted into larger crystal growing during annealing. All the phases formed after annealing at 700 °C remained present and variations in the quantity of the phases and crystal sizes at each annealing temperature was observed. The broad peaks observed after annealing can be explained to be due to strain.

Table 1 Average crystal size of the silicides, oxides and carbides calculated from the XRD patterns

Temp (°C)	W (nm)	W_5Si_3 (nm)	WC (nm)	W_2C (nm)	WO_3 (nm)	SiO_2 (nm)
As-deposited	37.6	74.1	45.9	—	65.2	—
700	73.5	83.9	294.4	19.7	70.7	43.8
800	165.8	200.4	125.3	128.2	103.4	105.7
900	161.7	210.0	185.7	164.9	123.5	128.7
1000	173.2	176.1	177.8	108.4	125.4	137.5

The W–Si–C system heat of formation for the phases formed is reported in ref. 23, 27 and 28. The system predicts the thermodynamically expected phases at different temperatures and those seen after conducting experiments. Different researchers have obtained different initial phases such as Geib *et al.*[22] who found WSi_2 and WC as the initial phases after deposition, Rogowski *et al.*[4] found both WSi_2 and W_5Si_3 after annealing (Ar ambient) at 700 °C as initial phases, Baud *et al.*[29] found W_5Si_3 and W_2C at 950 °C (vacuum) as the initial phases. This implies that the different sample preparation techniques used and annealing in different mediums lead to the formation of different phases. Using the Gibbs free energy and the Ellingham diagram, Seng and Barnes[27] calculated the kinetically favoured initial phases for temperature range between 300 K $\leq T >$ 970 K to be WSi_2 and WC. In our case WC was formed as also predicted by Seng, but the silicide (WSi_2) which is stable with SiC and carbide did not form. In our study, W_5Si_3 was the silicide that formed and not WSi_2. W_5Si_3 and WC are the two thermodynamically favoured phases based on heat of formation calculations.

In the study of W–SiC samples annealed in hydrogen ambient,[24] it was observed that phases present were W_5Si_3, WC and W, while at 800 °C to 1000 °C two additional phases appeared, that is, WSi_2 and W_2C. After vacuum annealing,[26] the phases which formed upon annealing at 700 °C and 800 °C were WO_2, WC, W and W_3C, while at 900 °C and 1000 °C WSi_2 and W_2C were the additional phases formed. In this study on Ar annealing, phases present after annealing from 700 °C to 1000 °C were WO_3, W_5Si_3, SiO_2, W_2C and WC.

3.3. SEM

For confirmation of the change in surface structure due to annealing in the W–SiC samples, SEM analysis was conducted. In Fig. 3, the SEM micrographs of W thin film deposited on 6H–SiC before and after annealing at 700 °C, 800 °C, 900 °C and 1000 °C for 1 hour in Ar ambient are depicted. The as-deposited sample shows a fairly flat surface of the W thin film, with very small grains (almost the same size) that are evenly distributed. This confirms the XRD analysis of the as-deposited results which indicated the formation of nano-sized particles in the as-deposited. Annealing at 700 °C and 800 °C leads to a major change in the surface morphology of the samples. The sample surface becomes crystalline at 700 °C and the crystals are of different sizes and shapes and are also randomly orientated. At 800 °C rod-like crystals of different sizes are observed with no preferred orientation. At both the temperatures, some of the crystals are protruding from the surface. The difference in surface morphology indicates that substantial reactions along with atomic migration in the W film surface took place during annealing at 700 °C and 800 °C.

Smith and Thompson,[30] investigated the effect of annealing in N_2 and Ar ambient of $W_{0.62}Si_{0.38}$ on Si. They co-sputtered W and Si on a Si substrate; they observed that annealing in argon results in the formation of large grains while in N_2 a smooth surface. The change in the surface structure of $W_{0.62}Si_{0.38}$ deposited on Si after annealing in argon which produced the highly rough surface was ascribed stress assisted growth which results into large columnar grains. In our results after annealing in argon ambient, a rough surface resulted due to reaction of W and SiC and might also be stress assisted growth.

Annealing at 900 °C and 1000 °C resulted in the crystals growing larger and stacked on top of each other with pores observed between the crystals. In the substrate surface between the pores small crystallites were observed to have formed. These results are in agreement with the XRD results where the increase in the intensity of most of diffraction peaks denoted that for those phases the average crystal sizes increased during annealing. These phases are most probably the large crystals observed in Fig. 3.

The average crystal sizes of the Ar annealed (from 700 °C to 1000 °C) W–SiC samples are larger and more randomly orientated when compared to vacuum annealed[26] and hydrogen annealed W–SiC samples.[24] A slow crystal growth in the form of grains was observed during annealing in hydrogen. Annealing in vacuum resulted in the formation of grains which changed with an increase in temperature to form crystals in the form of distinct islands (pores between the flat crystals). The formation of large crystals and spaces between crystals on the W–SiC surfaces was also observed on W–SiC samples annealed in vacuum.[26] These cavities are formed during the parasitic growth of crystallites and crystal surfaces at elevated temperatures. Parasitic growth follows Wulf's law[31] and is due to the feeding from crystal surfaces with lower surface energies to surfaces with higher surface energies, resulting in the former growing faster than the latter thereby exposing larger areas of crystal surfaces with lower surface energies. This leads to a minimisation of the Gibbs free energy of the system.

The different surface morphologies between the hydrogen and vacuum annealed surfaces were previously explained to be due to the reducing effect (*i.e.* removal of oxygen) of the hydrogen.[24] The different morphology of the Ar annealed samples can be explained in terms of a crystal growth model. Some gas atoms present in the annealing system can be physio-sorbed or chemi-sorbed on the crystallite surfaces in the layer and in the

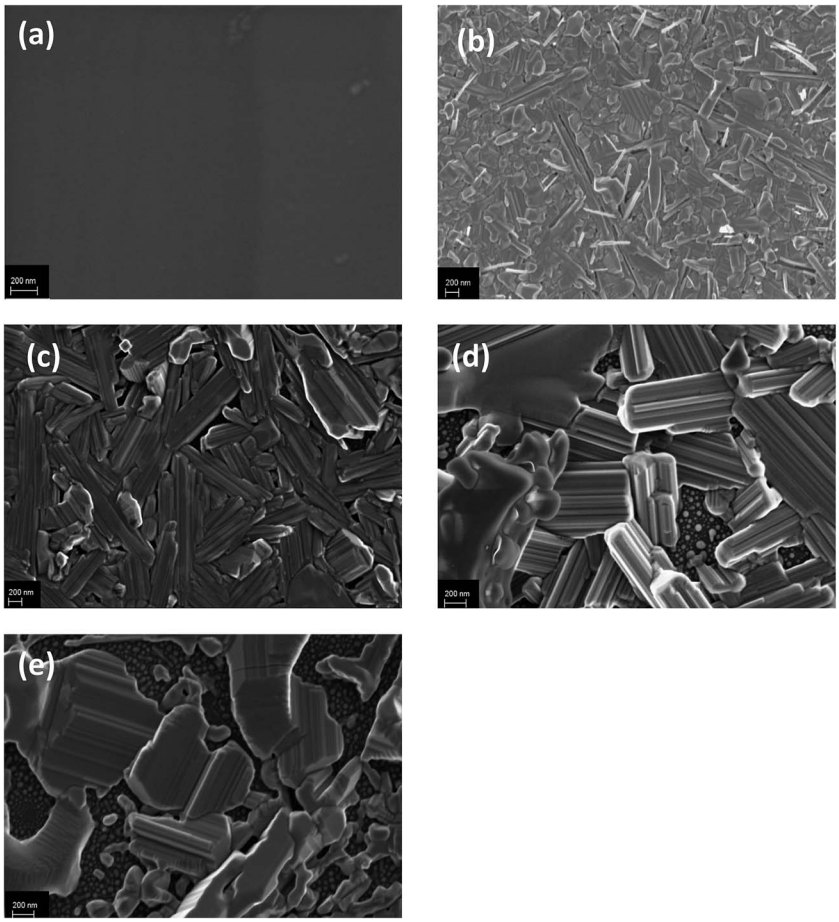

Fig. 3 SEM micrographs of (a) as-deposited W–SiC and Ar-annealed samples at (b) 700 °C, (c) 800 °C, (d) 900 °C and (e) 1000 °C for 1 hour.

reaction zone *via* cavities/opening in the layer during annealing. During vacuum annealing, reactive gases still present in the vacuum can stick to the surfaces of the crystallites. In fact, WO_3 was detected in those samples after annealing.[26] Hydrogen is a reacting gas which is commonly physio-sorbed or chemi-sorb on surfaces. According to the step-flow mechanism[32] of crystal growth, impurity atoms on the growth surfaces of crystallites inhibit the growth process of the crystallites. Based on this model, one can expect the hydrogen annealed samples to have smaller crystallites than the vacuum annealed samples – as was observed.[24,26] Because Ar is a noble gas with no chemi-sorption and little physio-sorption expected on the surfaces, the Ar annealed samples should have the largest crystallites – also observed in this study. This model of impurities sticking on the crystallites surface might also be the reason for the different phases being formed in the different annealing environments.

The presence of oxygen as an oxide might also be influencing the crystal growth. The growth rate in Ar annealed and vacuum annealed sample is high as compared to the hydrogen annealed samples which have a small quantity of oxygen. The quantity of oxygen in Ar annealed sample does not reduce, while in the vacuum annealed sample it reduces with annealing temperature. The quantity of oxygen present might be influencing the crystal growth observed.

Annealing in different environment was observed to produce different surface morphologies. The samples annealed in vacuum contained tungsten oxide nanowires, while the formation of small W grains is observed in the hydrogen annealed samples. Large crystals were observed on the surface of the argon annealed samples, clearly indicating the surface morphology dependence on annealing ambient. Annealing at 900 °C and 1000 °C indicates that the material crystallizes at a fast rate in an Ar ambient with the formation of large crystals with spaces in between them, while the vacuum annealed samples led to the formation of islands with holes in between, and an increase in the W grain size observed on the surface of H_2 annealed samples.

4. Summary

W thin films were deposited on 6H–SiC and annealed for 1 hour (each) in the temperature range 700 °C to 1000 °C in an argon ambient. The solid state interactions together with structural morphology were studied. RBS results of the as-deposited layer indicated the presence of unreacted W on SiC. Interdiffusion of W, O and SiC was observed to be taking place and it increased with increasing annealing temperature. The as-deposited GIXRD patterns showed broad peaks indicating that nano-sized particles

were formed after deposition. The new phases present were WO_3, W_5Si_3 and WC. The samples annealed at 700 °C resulted in the formation of W_2C and SiO_2 in addition to the phases observed in the as-deposited sample. Annealing from 800 °C to 1000 °C showed an increase in the GIXRD peak intensities of the phases formed without the introduction of new phases.

SEM micrographs showed a fairly uniform W thin film, with very small grains that were evenly distributed. An increase in the XRD peak intensity with an increase in temperature was observed, which was due to the growing of larger crystallites in the sample. SEM images also confirmed that upon annealing the surface crystals grew larger with increasing annealing temperatures. SEM images for the temperature range 800–1000 °C showed that the increase in crystal size was accompanied with an increasing number of cavities and with increasing cavity sizes.

Annealing in different atmospheres lead to different behaviour of the thin film W deposited on 6H–SiC. Annealing this system in a H_2 atmosphere resulted in relatively small crystallites. This is explained in terms of the sticking of impurities on the growth surfaces of the crystals using the step-flow model of crystal growth. The fact that large crystals were formed after annealing in an Ar ambient is similarly ascribed to fewer impurities in the Ar annealed samples as compared to the vacuum and H_2 annealed samples. Island formation on the surfaces (with pores between the crystals) of the Ar and vacuum annealed samples was influenced by the parasitic growth of crystallites following Wulf's law. The initial reaction temperature (from RBS) between the W layer and the SiC substrate was lower for the Ar and H_2 ambient annealed samples than for the vacuum annealed samples.

Acknowledgements

This work is based upon research supported by the National Research Foundation (NRF) (Grant number: 88661), South Africa. Any opinion, findings and conclusions or recommendations expressed in this work are those of the authors and the NRF do not accept any liability with regard thereto. T. T. Thabethe acknowledges the financial support from the NRF.

References

1 D. Ebbing and S. D. Gammon, *General Chemistry*, Charles Hartford, Belmont, USA, 9th edn, 2011.
2 Metalpedia.
3 J. Tan, Z. Zhou, M. Zhong, X. Zhu, M. Lei, W. Liu and C. Ge, *Phys. Scr.*, 2011, **T145**, 14055.
4 J. Rogowski and A. Kubiak, *Mater. Sci. Eng., B*, 2015, **191**, 57–65.
5 R. S. Okojie, L. J. Evans, D. Lukco and J. P. Morris, *IEEE Electron Device Lett.*, 2010, **31**, 791–793.
6 H. Kishimoto, T. Shibayama, T. Abe, K. Shimoda, S. Kawamura and A. Kohyama, *IOP Conf. Ser.: Mater. Sci. Eng.*, 2011, **18**, 162015.
7 J. B. Malherbe, N. G. van der Berg, R. J. Kuhudzai, T. T. Hlatshwayo, T. T. Thabethe, O. S. Odutemowo, C. C. Theron, E. Friedland, A. J. Botha and E. Wendler, *Nucl. Instrum. Methods Phys. Res., Sect. B*, 2016, **354**, 23–27.
8 E. Friedland, K. Gärtner, T. T. Hlatshwayo, N. G. van der berg and T. T. Thabethe, *Nucl. Instrum. Methods Phys. Res., Sect. B*, 2014, **332**, 415–420.
9 C. Guo, C. Zhang, L. He, B. Jin and N. Shi, *J. Mater. Sci. Technol.*, 2007, **23**, 677–684.
10 C. S. Houston, F. Proceedings, M. Command and F. Detrick, *1996 Twenty-Second International Power Modulator Symposium*, Palisades Institute for Research Services, Inc, Boca Raton, Florida, 1995.
11 F. Goesmann and R. Schmid-Fetzer, *Mater. Sci. Eng., B*, 1995, **34**, 224–231.
12 E. G. Njoroge, C. C. Theron, J. B. Malherbe and O. M. Ndwandwe, *Nucl. Instrum. Methods Phys. Res., Sect. B*, 2014, **332**, 138–142.
13 T. T. Hlatshwayo, J. B. Malherbe, N. G. Van Der Berg, L. C. Prinsloo, A. J. Botha, E. Wendler and W. Wesch, *Nucl. Instrum. Methods Phys. Res., Sect. B*, 2012, **274**, 120–125.
14 D. A. Petti, J. Buongiorno, J. T. Maki, R. R. Hobbins and G. K. Miller, *Nucl. Eng. Des.*, 2003, **222**, 281–297.
15 E. G. Njoroge, C. C. Theron, V. A. Skuratov, D. Wamwangi, T. T. Hlatshwayo, C. M. Comrie and J. B. Malherbe, *Nucl. Instrum. Methods Phys. Res., Sect. B*, 2016, **371**, 263–267.
16 E. G. Njoroge, C. C. Theron, T. T. Hlatshwayo and J. B. Malherbe, *RSC Adv.*, 2016, **6**, 68292–68301.
17 I. Tsiaoussis, N. Frangis, C. Manolikas and T. A. Nguyen Tan, *J. Cryst. Growth*, 2007, **300**, 368–373.
18 J. B. Malherbe, *J. Phys. D: Appl. Phys.*, 2013, **46**, 473001.
19 G. Matsuo, T. Shibayama, H. Kishimoto, K. Hamada and S. Watanabe, *J. Nucl. Mater.*, 2011, **417**, 391–394.
20 T. Hinoki, Y. Katoh, L. L. Snead, H.-C. Jung, K. Ozawa, H. Katsui, Z.-H. Zhong, S. Kondo, Y.-H. Park, C. Shih, C. M. Parish, R. A. Meisner and A. Hasegawa, *Mater. Trans.*, 2013, **54**, 472–476.
21 H. Kishimoto, T. Shibayama, K. Shimoda, T. Kobayashi and A. Kohyama, *J. Nucl. Mater.*, 2011, **417**, 387–390.
22 K. M. Geib, C. Wilson, R. G. Long and C. W. Wilmsen, *J. Appl. Phys.*, 1990, **68**, 2796–2800.
23 S. J. Son, K. H. Park, Y. Katoh and A. Kohyama, *J. Nucl. Mater.*, 2004, **329–333**, 1549–1552.
24 T. T. Thabethe, T. T. Hlatshwayo, E. G. Njoroge, T. G. Nyawo and J. B. Malherbe, *Vacuum*, 2016, **129**, 161–165.
25 L. R. Doolittle, *Nucl. Instrum. Methods Phys. Res., Sect. B*, 1985, **9**, 344–351.
26 T. T. Thabethe, T. T. Hlatshwayo, E. G. Njoroge, T. G. Nyawo, T. P. Ntsoane and J. B. Malherbe, *Nucl. Instrum. Methods Phys. Res., Sect. B*, 2016, **371**, 235–239.
27 W. F. Seng and P. A. Barnes, *Mater. Sci. Eng., B*, 2000, **72**, 13–18.
28 F. Goesmann and R. Schmid-Fetzer, *Mater. Sci. Eng., B*, 1997, **46**, 357–362.
29 L. Baud, C. Jaussaud, R. Madar, C. Bernard, J. S. Chen and M. A. Nicolet, *Mater. Sci. Eng., B*, 1995, **29**, 126–130.
30 P. M. Smith and M. O. Thompson, *MRS Proceedings*, 1988, **100**, 707–712.
31 G. Z. Wulf, *Krist. Mater.*, 1901, **34**, 449.
32 W. K. Burton, N. Cabrera and F. C. Frank, *Philos. Trans. R. Soc., A*, 1931, **243**, 299.